NUMERICAL SIMULATION AND ANALYSIS OF LITHIUM BATTERY HEAT DISSIPATION BASED ON MULTI-OBJECTIVE OPTIMIZATION

by

Mingxin ZHANG[a], Changfeng XUE[b*], Hailong QIU[b], and Xinwei JIN[a]

[a] College of Electrical Engineering, Yancheng Institute of Technology, Yancheng, Jiangsu, China
[b] College of Mathematics and Physics, Yancheng Institute of Technology, Yancheng, Jiangsu, China

Original scientific paper
https://doi.org/10.2298/TSCI220907208Z

In order to study the heat dissipation characteristics of lithium batteries, a staggered bi-directional flow cooling method is designed and numerical simulations are established using CFD in this paper with a circular battery as the research object. Since the optimal operating range of Li-ion battery is 293.15-313.15 K and the maximum temperature difference is not higher than 5 K, the maximum temperature and maximum temperature difference are selected as the optimized design objectives. Firstly, the temperature field of the round lithium battery with discharge multiplier 3C working at ambient temperature 308.15 K is studied, and an orthogonal test design is carried out for three factors: battery pack embedding distance, coolant flow rate and coolant temperature, and the best combination of orthogonal test is selected by extreme difference analysis and analysis of variance. Secondly, in order to further verify the heat dissipation efficiency of the battery pack, a back propagation neural network with multi-objective optimization algorithm is proposed, and the optimal heat dissipation method of the numerical simulation is obtained by parameter solution and simulation analysis using the parameter range of the orthogonal test as the constraints of the multi-objective optimization. The results show that this optimized way of battery pack heat dissipation has a significant improvement for the maximum temperature, and non-e of them will exceed its working range; compared with the 3.39 K obtained from the orthogonal test design, the maximum temperature difference of the battery pack calculated by the multi-objective optimization is 3.15 K, which is reduced by 7.08%.

Key words: *lithium batteries, numerical network, liquid cooling, orthogonal test, multi-objective optimization*

Introduction

With the gradual popularization of new energy vehicles, more and more electric vehicles are appearing in people's view, and automotive Li-ion batteries are developing rapidly and have the advantages of high energy density [1] and long cycle life [2]. However, Li batteries generate heat during operation, and if the internal cooling system cannot control the temperature of the battery pack itself and its temperature uniformity, the increase in battery pack temperature will directly affect its performance and service life [3]. If it is in a high temperature state for a long time, it may lead to thermal runaway, fire or even explosion, which may cause accidents or endanger personal safety [4]. Therefore, it is necessary to design a complete Li-ion

* Corresponding author, e-mail: cfxue@163.com

battery heat dissipation system to not only avoid high maximum battery pack temperature but also to ensure the temperature uniformity of the battery pack [5]. Usually, the optimal operating range of Li-ion batteries is 20-40 °C, with a maximum temperature difference of no more than 5 °C [6].

The mainstream battery cooling methods include air cooling, liquid cooling, and PCM cooling [7]. Liquid cooling is the most common cooling method and is widely used due to its obvious cooling efficiency and sophisticated control methods [8]. Liquid cooling is a cooling plate or cooling tube with internal flow channels in contact with the cell, which is cooled by a coolant with strong heat exchange efficiency [9]. At present, most scholars have carried out numerical simulation and structural optimization of battery cooling [10], Huang *et al*. [11] designed a PCM-water jacket type liquid cooling structure and investigated the optimal flow channel structure for PCM cooling model at different battery spacing. Feng *et al.* [12] proposed a new honeycomb cooling power battery pack and analyzed the effects of coolant flow and temperature on the heat dissipation performance of the battery pack, with significant variation in the maximum temperature of the battery pack and stable temperature uniformity. Xu *et al.* [13] designed a snake-shaped cooling channel and a *U*-shaped cooling channel, and proposed an optimized design model based on an improved particle swarm algorithm, which resulted in a significant reduction of the maximum temperature difference of the battery pack. Liu *et al*. [14] designed a new simulated fin-vein runner cooling plate, simulated two heat dissipation methods of bionic fin-vein runners and inlet and outlet positions, and analyzed the effects of parameters such as adjacent coolant flow direction and runner slot depth of the battery pack on cooling plate heat dissipation, which provided a reference for battery pack heat dissipation performance and low energy consumption.

However, most researchers have optimized the battery pack structure under different influencing factors [15], such as the type of runners, the number of cooling plates*, etc.*, while the main parameters affecting heat dissipation and the optimal combination of methods have been less studied. The main feature of this paper was to design a staggered bi-directional flow cooling method with the maximum temperature and maximum temperature difference as the target, and to analyze the best combination of orthogonal tests by orthogonal test design with three factors and four levels. Then, through multi-objective optimization, the optimal solution within the parameter range is found to obtain a better cooling effect while ensuring the uniformity of cell temperature distribution.

Model

Establishment of geometric model

The object of this paper is a 2 Ah 18650 type Li battery, which is simplified as a cylinder with a diameter of 18 mm and a height of 65 mm. The whole battery pack consists of 50 cell units, cooling plate and coolant, where the cell units are aligned in 5 rows and 10 columns with a row spacing of 22 mm and a column spacing of 23 mm and embedded in the cooling plate. The cooling runner is 3 mm wide and 216 mm long. The cooling plate adopts a staggered bi-directional flow inside, *i.e.* the upper half is the inlet end and the lower half is the outlet end, and the inlet and outlet are arranged in opposite directions between adjacent cooling plates; the coolant flows in from the inlet end, passes through the cooling plate for heat exchange with the battery pack, and then flows out from the outlet end to provide heat dissipation for the battery pack. The schematic picture of battery pack geometry model structure, the coolant flow direction picture, the distance of the embedded cooling plate of the battery and the schematic diagram of the cooling plate structure are shown in figs. 1 and 2.

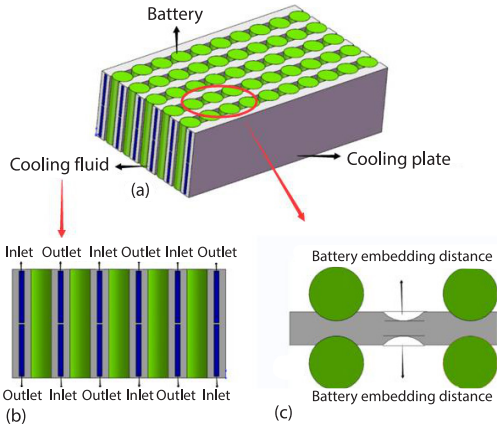

Figure 1. (a) schematic picture of battery pack geometry model structure, (b) coolant flow direction picture, and (c) battery embedded cooling plate distance

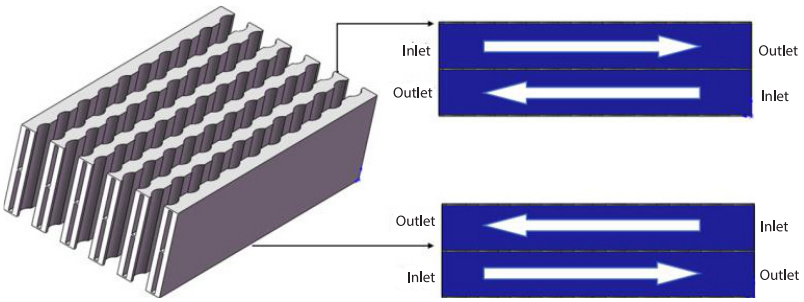

Figure 2. Schematic diagram of cooling plate structure

Mathematical modelling

Since the thermal conductivity of the battery monomer is anisotropic, the differential equation for the thermal conductivity of the battery is:

$$\rho c_p \frac{\partial T}{\partial t} = \lambda_x \frac{\partial^2 T}{\partial x^2} + \lambda_y \frac{\partial^2 T}{\partial y^2} + \lambda_z \frac{\partial^2 T}{\partial z^2} + q \tag{1}$$

where ρ [kgm^{-3}] is the battery density, c_p [Jkg^{-1}K^{-1}] – the specific heat capacity of the battery, λ_x, λ_y, and λ_z [Wm^{-1}K^{-1}] are the thermal conductivity in each direction, T [K] – the temperature of the battery, and q [Wm^{-3}] – the heat generation rate per unit volume of the battery.

Since it is difficult to calculate the heating rate of a battery during discharge, the mathematical model of heat generation rate established by Bernardi [16] is often used to calculate it, considered the battery as a uniform heat source whose temperature varies with time:

$$q = \frac{I}{V}\left[\left(E_{\text{oc}} - E\right) + T\frac{\mathrm{d}E_{\text{oc}}}{\mathrm{d}T}\right] \tag{2}$$

where I [A] is the battery current, E_{oc} [V] – the open-circuit voltage, E [V] – the actual working voltage of the battery, $\mathrm{d}E_{\text{oc}}/\mathrm{d}T$ – the temperature entropy coefficient, and V [m^3] – the volume of the battery.

There is a natural-convection between the outer surface of the battery and the ambient temperature:

$$-\lambda_{\text{w}}\left(\nabla T_{\text{w}}\right) = h\left(T_{\text{w}} - T_0\right) \tag{3}$$

where λ_w is the thermal conductivity of battery pack surface and T_w [K] – the temperature of the outer surface of the battery string.

The flow state of coolant during simulation can be obtained by Reynolds number:

$$\mathrm{Re} = \frac{\rho v L}{\mu} \tag{4}$$

where L [m] is the characteristic length of coolant.

Condition assumptions

Due to the complexity of the actual heat generation of the battery pack, which will be affected by the current, internal resistance and other factors, in order to ensure the accuracy of the simulation, this paper made the following assumptions on the battery pack model:

– The internal heat radiation of the battery pack is not considered.
– The material of the battery is isotropic, with uniform internal heat generation and constant thermal conductivity.
– The surface temperature of the battery is uniform and the heat transfer coefficient is consistent with the environment in all directions.

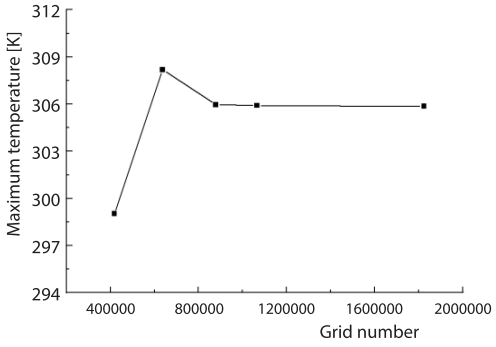

Figure 3. Independence test of grid number

Grid independence test

Due to the complex internal structure of the battery pack, the independence of the grid needs to be verified [17] to ensure the influence of the number of grids on the results and to improve the accuracy of the calculation. In this paper, an unstructured grid with boundary-layers is used, and five different numbers of grids, 417949, 636975, 877479, 1065853, and 1824116, are used for simulation under 3C discharge, as shown in fig. 3. When the grid reaches 877479, the highest temperature change does not exceed 0.1 K after increasing the number of grids again. For the accuracy of the simulation, the number of grids is set to 1065853 for calculation.

Simulation condition setting

Ethylene glycol is usually dissolved in water as an organic compound because of its colorless, odorless and low volatility characteristics [18]. In this paper, 50% volume fraction of aqueous ethylene glycol solution is selected as the cooling fluid and aluminum plates were used as cooling plates for the battery pack with the thermal physical parameters shown in tab. 1.

Table 1. Thermal physical parameters of materials

Material	ρ [kgm^{-3}]	c_p [Jkg^{-1}K^{-1}]	λ [Wm^{-1}K^{-1}]	μ [Pa·s]
Battery	2018	1282	0.9/0.9/2.7	–
Aluminum	2719	871	3319	–
Cooling fluid	1068.75	3319	0.387	0.00294

The velocity inlet and pressure outlet are selected for the coolant, and the Reynolds number calculated in this paper is less than 2300, so the laminar flow is used for the coolant

model. The initial environment is set to 308.15 K (35 °C), and convective heat transfer is carried out between the cell surface and the environment, and the heat transfer coefficient is taken as 5 W/m^{2}K.

In this paper, a transient solver is used for the solution, in which the momentum equation is solved using the semi-implicit method for pressure linked equations (SIMPLE) algorithm based on pressure-velocity coupling, and the discrete solution equations for pressure, momentum and energy are chosen in second-order windward format. To ensure the accuracy of the calculation scheme as much as possible, the residual values of the continuity equation, velocity and energy equations are set to 10^{-6}. The heat generation of the battery pack under 3C power discharge is simulated, and the external energy power of the battery pack was set to 42400 W/m^3 as the internal heat source [19]. The discharge time is set to 1200 steps and the step size is set to 1 second, with 20 iterations per unit step.

Orthogonal test design and analysis

Orthogonal test design

The method of interlaced bi-directional flow cooling can improve the temperature uniformity of the battery pack, but there are many other factors that affect the temperature variation of the battery pack. To ensure the good performance and lifetime of the battery pack, this paper conducted an orthogonal test by varying three factors: the distance of the battery embedded in the cooling plate, the coolant flow rate and the coolant temperature. The orthogonal test design is designed to obtain representative data by reducing the number of tests [20], so that the maximum temperature and maximum temperature difference of the battery pack are in the optimal temperature range. The maximum temperature difference of the test target should be less than 5 K, and the maximum temperature should be controlled between 293.15 K and 313.15 K.

Firstly, for the three influencing factors, a control variable method is used to simulate the battery pack separately and calculate its temperature distribution at a discharge time of 100 seconds. Figure 4(a) shows the maximum temperature and maximum temperature difference at 0.003 m/s, 0.01 m/s, and 0.02 m/s coolant flow rates when the coolant temperature is 25 °C and the battery pack embedding distance is 3 mm. The maximum temperature gradually decreases with the increase of the flow rate, and the maximum temperature difference first rises significantly and then changes less, and when the flow rate reaches a certain value, the maximum temperature difference no longer produces significant changes.

Figure 4(b) indicates the maximum temperature and maximum temperature difference at coolant temperature values of 20 °C, 25 °C, and 30 °C for a coolant flow rate of 0.01 m/s and battery pack embedding distance of 3 mm. The maximum temperature continues to rise with the increase of coolant temperature and shows a positive correlation, while the maximum temperature difference decreases significantly with the increase of coolant temperature and shows a negative correlation.

Figure 4(c) shows the maximum temperature and maximum temperature difference of the battery pack at different embedding distances when the coolant temperature is 25 °C and the coolant flow rate is 0.01 m/s. Both the maximum temperature and maximum temperature difference of the battery pack decrease with the increase of embedding distance, however, the changes of these two indicators do not occur significantly when a certain value is reached.

In order to facilitate the processing of the test data, the same number of levels are selected for each factor, where the distance of the battery embedded in the cooling plate, the flow rate of the coolant and the temperature of the coolant are controlled at 1~4 mm, 0.003~0.02 m/s, and 20~30 °C. For the accuracy of the results and the number of tests, four levels are

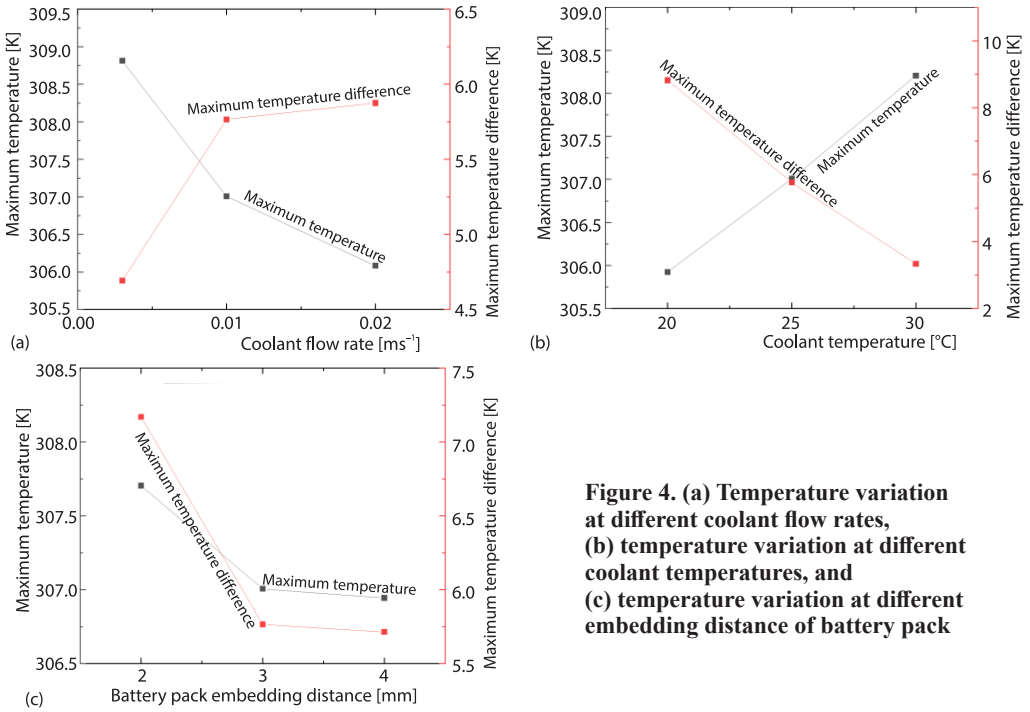

Figure 4. (a) Temperature variation at different coolant flow rates, (b) temperature variation at different coolant temperatures, and (c) temperature variation at different embedding distance of battery pack

selected for each of the three parameters in this test, and an orthogonal table was chosen, as shown in tab. 2. For the convenience of description, A, B, and C are used to denote the battery embedding distance, coolant flow rate and coolant temperature.

Table 2. Factor levels table

Factors	Level 1	Level 2	Level 3	Level 4
A [mm]	1	2	3	4
B [ms^{-1}]	0.003	0.005	0.01	0.02
C [°C]	20	24	27	30

The L16(4^5) orthogonal test table is chosen for the scheme design, without considering the interaction between the factors, and 16 tests were to be performed, in which the highest temperature and the maximum temperature difference during the discharge of the battery pack were used as the test results. Fluent was used for numerical simulation of all schemes, and the schemes, factors and results of the orthogonal test are filled in tab. 3.

From the analysis of the results of the orthogonal table, it can be seen that the maximum temperature of the battery pack is controlled below 313.15 K (40 °C) under the design scheme of each combination of factor levels, which achieved the best working range of the battery pack and has a good temperature control effect. However, the maximum temperature difference in the table varies more obviously, so the analysis of the orthogonal test is mainly based on the maximum temperature difference as the test index.

Orthogonal test analysis

To investigate the combination of factor levels affecting the maximum temperature difference, the results of the experiment were analyzed using analysis of variance and range

Table 3. Orthogonal test scheme and simulation results

Noumbers	A [mm]	B [ms^{-1}]	C [°C]	T_{max} [K]	ΔT_{max} [K]
1	1	0.003	20	309.14	10.88
2	1	0.005	24	308.96	9.09
3	1	0.010	27	308.81	7.61
4	1	0.020	30	308.80	5.48
5	2	0.003	24	309.03	6.65
6	2	0.005	20	308.74	9.28
7	2	0.010	30	308.76	4.14
8	2	0.020	27	308.54	6.62
9	3	0.003	27	308.96	4.59
10	3	0.005	30	308.85	3.43
11	3	0.010	20	308.53	9.19
12	3	0.020	24	308.47	7.70
13	4	0.003	30	309.09	3.39
14	4	0.005	27	308.74	4.39
15	4	0.010	24	308.55	6.38
16	4	0.020	20	308.44	9.56

Table 4. Analysis of extreme differences table

Parameter	A	B	C
Mean 1	8.268	6.363	9.727
Mean 2	8.672	6.547	7.454
Mean 3	6.226	6.832	5.804
Mean 4	5.915	7.339	4.096
Range R	2.353	0.976	5.631

analysis to obtain the importance and magnitude of the effect of each factor level. In tab. 4, the mean value is the average of the maximum temperature difference of each factor at the corresponding four levels. The extreme difference, R, is the difference between the maximum mean value and the minimum mean value in the same factor. The size of the extreme difference represents the importance of the corresponding factor on the test results, and the larger the value of the extreme difference, the greater the influence of the factor on the test results. Conversely, the smaller the influence on the results.

From tab. 4, it can be seen that $R_C > R_A > R_B$ indicated that the degree of influence of each factor on the maximum temperature difference of the battery pack from high to low is coolant temperature, battery pack embedding distance and coolant flow rate. Since the mean value represented the degree of influence of the factors on the maximum temperature difference, the optimization levels in factors A, B and C in the table are classified as 4, 1, and 4, the best optimized combination was $C_4A_4B_1$. In order to further verify the influence of the factors on the maximum temperature difference of the battery pack, the results of the orthogonal test were analyzed by analysis of variance, as shown in tab. 5.

Analysis of variance can get the influence of each factor on the test index by significance, and the smaller the significance coefficient represented the more significant influence of its factors. In tab. 5, the influence of coolant temperature on the maximum temperature difference of the battery pack is the most obvious, followed by the embedding distance of the battery pack, and the coolant flow rate had the least influence. In summary, the results obtained by analysis of variance and range analysis are consistent, which verified the accuracy of the orthogonal test.

Table 5. Analysis of variance table

Factors	Sum of square	DoF	Mean square	*F*	Significance
A	13.115	3	4.372	16.656	0.057
B	2.176	3	0.725	2.763	0.266
C	69.188	3	23.063	87.866	0.011
Error	0.787	3	0.262	–	–

Through the aforementioned analysis, the optimal solution for the maximum temperature difference of the battery pack is $C_4A_4B_1$, which is the orthogonal test design scheme 13, where the embedding distance of the battery pack is 4 mm, the coolant flow rate is 0.003 m/s, and the coolant temperature is 30 °C. The numerical simulation temperature change curve and the final temperature distribution cloud at 1200 seconds of discharge are shown in figs. 5 and 6.

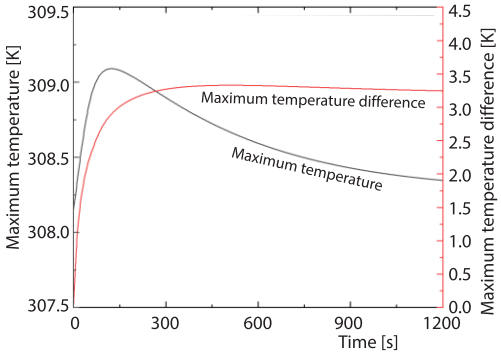

Figure 5. Battery pack temperature change curve

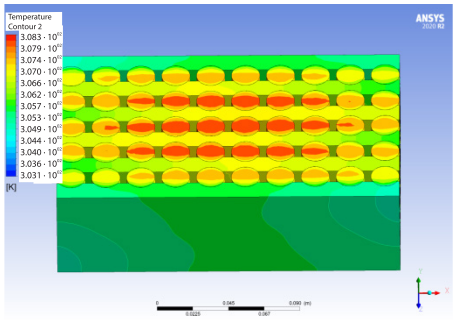

Figure 6. Temperature distribution cloud map

The maximum temperature and the maximum temperature difference are in the best working range of the battery pack. It can be seen from fig. 6 that the high temperature range is mainly distributed in the center of the battery pack, which is due to the location around the battery pack has better cooling conditions, with the continuous discharge of the battery pack, the temperature difference between the edge and the center gradually increases, and the temperature rise is higher when the coolant reaches the center, and the heat is too late to be transferred outward, so the battery pack needs to be further optimized.

Multi-objective optimization algorithm

Back propagation neural network

Back propagation neural networks are multilayer feedforward networks trained according to the error back propagation algorithm, which can approximate non-linear functions with arbitrary accuracy and can input and output data under uncertain mathematical mapping

relationships. By learning and training the non-strict mapping relationship between input and output data through neural networks, it had the ability to establish good non-linear relationships and achieved output data result prediction.

Table 6. Neural network test data

Numbers	A [mm]	B [ms^{-1}]	C [°C]	T_{max} [K]	ΔT_{max} [K]
17	1.2	0.007	28.4	308.89	5.54
18	1.5	0.012	22.3	308.57	10.35
19	1.8	0.009	24.5	308.62	7.54
20	2.5	0.004	25.7	308.89	5.73
21	3.4	0.007	26.4	308.64	5.05
22	3.5	0.003	26.76	308.93	4.42

In this paper, the optimization of three factors on the two objectives of maximum temperature and maximum temperature difference of the battery pack is investigated. Firstly, orthogonal tests are combined with back propagation neural network, and 16 sets of orthogonal tests are selected as the training set of the neural network, and any six different sets of parameters were taken in the range of variable values, as shown in tab. 6. Then the numerical simulation is performed by FLUENTl, and the simulation results are used as the test data set of the neural network.

The back propagation neural network consists of three parts: input layer, hidden layer and output layer, and two sets of neural network prediction models were established, and each set of models has three input layer neurons, which are battery pack embedding distance, coolant flow rate and coolant temperature. Each group of output layer neurons is 1, which are maximum temperature and maximum temperature difference. Since there is no corresponding mathematical formula to determine the specific number of implied layer neurons, this paper predicted the results by neural network and sets the number of implied layer neurons to 7.

The correlation analysis regression curves and error histograms for the maximum temperature and maximum temperature difference were obtained by validating the neural network model, and figs. 7 and 8 show how well the network output fits the training, validation, and test sets. The prediction model fitted by the neural network between the input and output data will be used as the objective function of the multi-objective optimization algorithm.

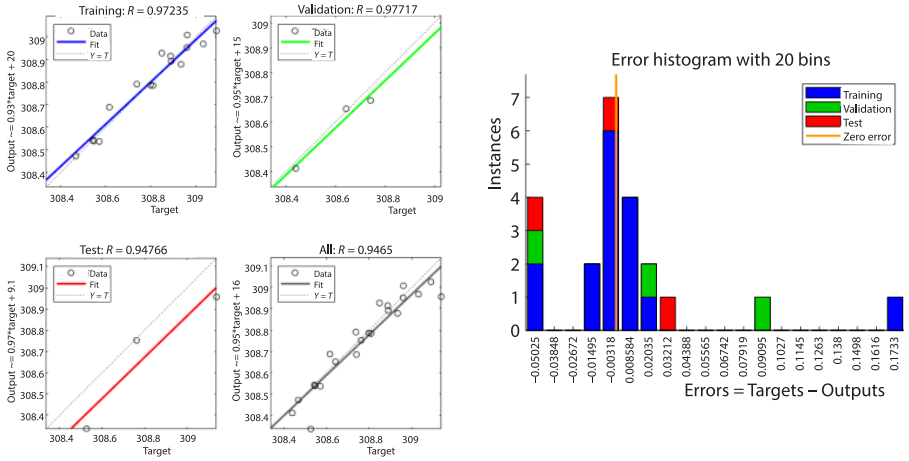

Figure 7. Correlation analysis and error histogram of the highest temperature training

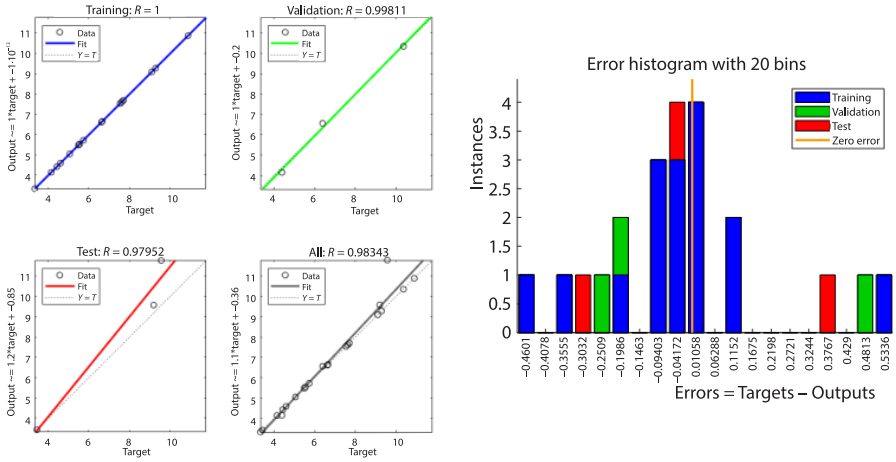

Figure 8. Correlation analysis and error histogram of the highest temperature difference training

In the figs. 7 and 8, the correlation analysis values of 0.97235, 0.97717, and 0.94766 for the training set, validation set and test set for the maximum temperature and 1, 0.99811, and 0.97952 for the training set, validation set and test set for the maximum temperature difference. In the error histogram, it can be seen that the errors of [0.05025, 0.1733] for the maximum temperature model and [0.4601, 0.5336] for the maximum temperature difference model are within the acceptable range, and all these results prove that the training data set is suitable and the model is valid.

Multiple objective optimization

The trained neural network model is used as the objective function of the Pareto multi-objective optimization algorithm, and the battery pack embedding distance, coolant flow rate and coolant temperature are used as the study objects. For the parameters in the orthogonal experimental design as design variables, and the design range is the range of the variables, the mathematical description is expressed:

$$\begin{aligned} &\min F(x) = \left[f_1(x), f_2(x)\right] = \left[y_1, y_2\right] \\ &s.t.\ \ x = \left\{\left(x^1, x^2, x^3\right) \middle| x^1 \in [1,4], x^2 \in [0.003, 0.02], x^3 \in [20,30]\right\} \end{aligned} \tag{5}$$

where x^1, x^2 and x^3 are the embedding distance, coolant flow rate and coolant temperature of the battery pack; $f_1(x)$, $f_2(x)$ are the maximum temperature and maximum temperature difference of the battery pack and y_1, y_2 are the prediction models obtained from the neural network.

For the two optimization objectives of this paper: minimization of the maximum battery pack temperature and minimization of the maximum temperature difference. The x_1 dominates the x_2 in the case of satisfying the following equation, which proves the superiority of x_1 over x_2, as expressed:

$$\begin{aligned} &\forall\left[f_1(x_1) \le f_1(x_2) \wedge f_2(x_1) \le f_2(x_2)\right] \\ &\exists\left[f_1(x_1) < f_1(x_2) \wedge f_2(x_1) < f_2(x_2)\right] \end{aligned} \tag{6}$$

Throughout the design variable interval, all solutions that satisfy the previous equations are Pareto non-inferior solutions and have no superiority or inferiority.

The Pareto algorithm program was written using MATLAB to optimize the maximum temperature and maximum temperature difference of the battery pack. The initial parameters are set the population size is 50, the optimal individual coefficient is 0.4, and the maximum number of evolutions is 200. Finally, the optimized Pareto optimal solution is plotted as the Pareto front surface shown in fig. 9.

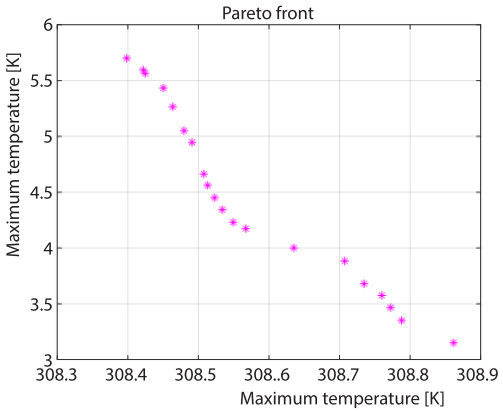

Figure 9. Pareto optimal solution chart

The horizontal co-ordinate indicates the maximum temperature of the battery pack and the vertical co-ordinate indicated the maximum temperature difference of the battery pack. Since the maximum temperature of the battery pack is in the optimal operating range during the discharge process, the main bias is to minimize the maximum temperature difference, the minimum longitudinal co-ordinate value of the Pareto front surface. The optimal solution is (308.86 K, 3.13 K), which corresponded to the battery pack embedding distance, coolant flow rate and coolant temperature of 3.954 mm, 0.0059 m/s, and 29.978 °C.

The parameters in the optimal solution are substituted into FLUENAT for numerical simulation, and the maximum temperature and maximum temperature difference obtained are 308.87 K and 3.15 K, which are basically consistent with the Pareto optimal solution. The battery pack temperature change curve and the final temperature distribution cloud are shown in figs. 10 and figs. 11.

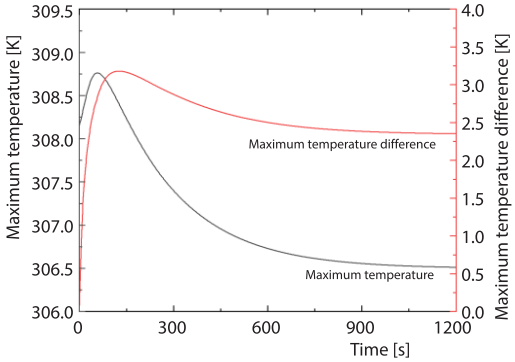

Figure 10. Battery pack temperature change curve

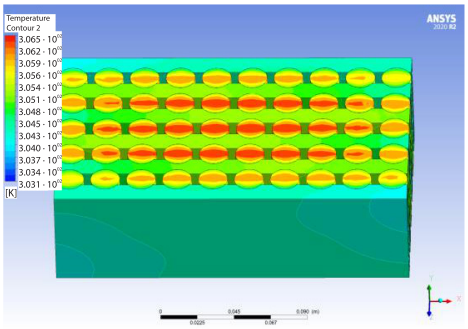

Figure 11. Temperature distribution cloud map

From figs. 10 and 11, it can be seen that with the Pareto optimal solution, the temperature difference of the battery pack increases and then decreases gradually during the 1200 seconds discharge time, where the maximum temperature difference is 3.15 K, which is 7.08% lower than the maximum temperature difference of 3.39 K of the best combination of the orthogonal test design. The temperature difference at the termination moment is 2.35 K, which is 27.7% lower than the final temperature difference of the orthogonal test, and has a very obvious improvement. The maximum temperature curve rises first and then decreases, and is much lower than the initial ambient temperature. Compared with the data from the orthogonal test, the temperature value of the battery pack is more uniform and the maximum temperature is lower.

Therefore, it can be proved that this optimization method has a more obvious improvement on the heat dissipation of the Li battery pack.

Conclusion

In this paper, the maximum temperature and the maximum temperature difference are used as the optimization objectives, and the staggered bi-directional flow cooling method is used to cool the battery pack, and the effects of embedding distance, coolant temperature and coolant flow rate on the temperature control of the battery pack are analyzed, and the following conclusions are drawn. The cooling effect of the staggered bi-directional flow design is relatively obvious, and the optimal combination of the three factors can be designed by orthogonal tests, however, the maximum temperature is concentrated in the center of the battery pack, and the heat dissipation effect needs to be improved. So again using multi-objective optimization combined with back propagation neural network, the Pareto optimal solution set can be obtained with the maximum temperature difference as the main factor, and the result obtained, compared with the optimal combination of orthogonal test, the maximum temperature difference is reduced from 3.39-3.15K, which is 7.08%. The final temperature difference is reduced from 3.25-2.35 K, which is 27.7%. It can increase the maximum temperature of the battery pack and improve the temperature uniformity of the whole battery pack.

References

[1] Cui, Z. H., *et al*., A Combined State-of-Charge Estimation Method for Lithium-Ion Battery Using an Improved BGRU Network and UKF, *Energy*, *259* (2022), 124933
[2] Cui, Z. H., *et al.*, A Hybrid Neural Network Model with Improved Input for State of Charge Estimation of Lithium-Ion Battery at Low Temperatures, *Renewable Energy*, *198* (2022), Oct., pp. 1328-1340
[3] Yu, H., Mao, B., Numerical Analysis and Optimization of Thermal Performance of Lithium Battery Pack Based on Air-Cooling Strategy, *Thermal Science*, *26* (2022), 5B, pp. 4249-4258
[4] Qi, W. J., *et al*., Thermal Management of Power Battery Based on Flexible Swiss Roll Type Liquid Cooling Micro-Channel, *Applied Thermal Engineering*, *219* (2023), 119491
[5] Yue, Q. L., *et al*., Pack-Level Modelling of a Liquid Cooling System for Power Batteries in Electric Vehicles, *International Journal of Heat and Mass Transfer*, *192* (2022), 122946
[6] Wang, Y., *et al*., Optimization of Liquid Cooling Technology for Cylindrical Power Battery Module, *Applied Thermal Engineering*, *162* (2019), 114200
[7] Wang, H. T., *et al*., Cooling Capacity of a Novel Modular Liquid-Cooled Battery Thermal Management System for Cylindrical Lithium-Ion Batteries, *Applied Thermal Engineering*, *178* (2020), 115591
[8] Kong, D. P., *et al*., A Novel Battery Thermal Management System Coupling with PCM and Optimized Controllable Liquid Cooling for Different Ambient Temperatures, *Energy Conversion and Management*, *204* (2020), 112280
[9] Jang, D. S., *et al*., Performance Characteristics of a Novel Heat Pipe-Assisted Liquid Cooling System for the Thermal Management of Lithium-Ion Batteries, *Energy Conversion and Management*, *251* (2022), 115001
[10] Ding, Y. Z., *et al*., Parameters of Liquid Cooling Thermal Management System Effect on the Li-Ion Battery Temperature Distribution, *Thermal Scienc*e, *26* (2021), 1B, pp. 567-577
[11] Huang, J. H., *et al*., Simulation Analysis of Thermal Management of Cylindrical Lithium-Ion Battery Pack with Phase Change Material Coupled with Water Jacketed Liquid Cooling Structure, *Energy Storage Science and Technology*, *10* (2021), 4, pp. 1423-1431
[12] Feng, N. L., *et al*., Study on Heat Transfer Characteristics of a New Honeycomb Liquid-Cooled Power Cell Module, *Journal of Chemical Engineering*, *70* (2019), 05, pp. 1713-1722
[13] Xu, H. W., *et al*., Optimization of Liquid Cooling and Heat Dissipation System of Lithium-Ion Battery Packs of Automobile, *Case Studies in Thermal Engineering*, *26* (2021), 101012
[14] Liu, X. X., *et al*., Liquid-Cooled Heat Dissipation of Lithium-Ion Battery Pack Based on Bionic Fin-vein Flow Channel Cold Plate, *Energy Storage Science and Technology*, *06* (2021), 70, pp. 2095-4239
[15] Sun, Y. X., Li, K. Q., Study on Heat Transfer Characteristics of Honeycomb Liquid-Cooled Lithium Battery Module, *Thermal Science*, *26* (2022), 5B, pp. 4285-4299

[16] Bernardi, D., *et al*., A General Energy Balance for Battery Systems, *Journal of The Electrochemical Society*, *132* (1985), 2113792
[17] Akbarzadeh, M., *et al.*, A Novel Liquid Cooling Plate Concept for Thermal Management of Lithium-Ion Batteries in Electric Vehicles, *Energy Conversion and Managemen*t, *231* (2021), 113862
[18] Guo, R., Li, L., Heat Dissipation Analysis and Optimization of Lithium-Ion Batteries with a Novel Parallel-Spiral Serpentine Channel Liquid Cooling Plate, *International Journal of Heat and Mass Transfer*, *189* (2022), 01, 122706
[19] Su, S. S., *et a*l., Multi-Objective Design Optimization of Battery Thermal Management System for Electric Vehicles, *Applied Thermal Engineering*, *196* (2021), 117235
[20] Ke, J., *et al*., Application of GA and BP Neural Network in Battery Heat Dissipation, *Mechanical Design and Manufacture*, *11* (2019), pp. 196-199

Paper submitted: September 17, 2022
Paper revised: October 12, 2022
Paper accepted: Decembr 1, 2022